



# The composition of Ni-Mo phases obtained by $\text{NiMoO}_x\text{-SiO}_2$ reduction and their catalytic properties in anisole hydrogenation



A.A. Smirnov<sup>a,\*</sup>, S.A. Khromova<sup>a,b</sup>, D.Yu. Ermakov<sup>a</sup>, O.A. Bulavchenko<sup>a,b</sup>, A.A. Saraev<sup>a,b</sup>, P.V. Aleksandrov<sup>a</sup>, V.V. Kaichev<sup>a,b</sup>, V.A. Yakovlev<sup>a,b,c</sup>

<sup>a</sup> Boreskov Institute of Catalysis SB RAS, Lavrenteva Ave., 5, 630090 Novosibirsk, Russia

<sup>b</sup> Novosibirsk State University, Pirogova Str. 2, 630090 Novosibirsk, Russia

<sup>c</sup> UNICAT Ltd., Lavrentieva Ave. 5, 630090 Novosibirsk, Russia

## ARTICLE INFO

### Article history:

Received 27 July 2015

Received in revised form 15 January 2016

Accepted 19 January 2016

Available online 21 January 2016

### Keywords:

Ni-Mo alloys

Hydrodeoxygenation

Hydrogenation

Anisole

NiMo-based catalysts

## ABSTRACT

The specific features of the formation of nickel- and molybdenum-containing phases during the reduction of the oxide precursor of the  $\text{NiMoO}_x\text{-SiO}_2$  catalyst with hydrogen at three different temperatures (470, 570, and 750 °C) were studied. The reduction behavior was investigated and the reduction temperature of oxide forms was determined with the use of the methods of temperature-programmed reduction, X-ray diffraction analysis, and X-ray photoelectron spectroscopy. It was shown that, at a reduction temperature from 470 to 570 °C, one can observe the formation of  $\text{NiMoO}_x$  particles with the  $\text{NiO}$ -type structure, Ni-Mo alloys of different composition, and  $\text{MoO}_2$ , which pass into the metallic phases Mo,  $\text{Ni}_3\text{Mo}$ , and  $\text{Ni}_x\text{Mo}_{1-x}$  at 750 °C. Nickel located at the surface is completely reduced to the metallic state in the temperature range of 300–750 °C, the Mo° content increases with the growing of treatment temperature and reaches 100% at 750 °C. Based on the data obtained, a reduction scheme for the catalytic system is proposed. The catalytic properties of the systems obtained are studied in the anisole hydrogenation reaction at a temperature of 300 °C and a hydrogen pressure of 6 MPa. The results of catalytic experiments showed that the 750-NiMo-SiO<sub>2</sub> catalyst possesses the highest specific activity in the anisole hydrogenation, which is probably due to the complete reduction of nickel oxide forms and molybdenum to metallic forms, which are highly active in the hydrogenation of C=O bonds and aromatic rings. The highest selectivity in the formation of oxygen-free products can be attributed to the catalysts reduced at 470–570 °C and whose active component contains coordinatively unsaturated molybdenum atoms. The most stable during the thermal treatment in acetic acid is the 750-NiMo-SiO<sub>2</sub> catalyst, which can be explained by the fact that it contains Ni-Mo alloys highly stable in the acid medium.

© 2016 Elsevier B.V. All rights reserved.

## 1. Introduction

An interest in the alternative energy sources, particularly in the alternative fuels, increases every year, which is primarily due to such factors as rising prices for oil products and decreasing stocks of natural resources. This is why more and more attention has recently been paid to renewable and cheap raw materials, for example, biomass can act as a partial or complete replacement of the natural oil. One of the most common ways of biomass treatment is fast pyrolysis that allows obtaining high product yields at high heating rates and short contact times [1]. However, the multi-component composition and the high oxygen content of up to 40% in the mate-

rial obtained by this method make it impossible to use the final treatment products as motor fuels without the use of an additional step, which is hydrotreating. The main objectives of this process are to reduce the oxygen content by the hydrodeoxygenation (HDO) and to increase the hydrogen content by means of the hydrogenation (HYD). Since the study of the pyrolysis oil hydrotreating process is very difficult due to the diversity of the composition of this raw material, so most of the works on the hydrodeoxygenation are devoted to studying the process not with real pyrolysis oil, but with its model compounds [2–4] or their mixtures [5–8]. One of the simplest oxygen-containing model compounds is anisole, which was studied in a number of articles [9–11]. Due to its simple structure and a small amount of derivatives, it is also well-suited for studying the kinetics of the process [12].

The most frequently examined HDO catalysts commercially used for petroleum hydrotreatment products are  $\text{NiMo}/\text{Al}_2\text{O}_3$  and

\* Corresponding author.

E-mail address: [asmirnov@catalysis.ru](mailto:asmirnov@catalysis.ru) (A.A. Smirnov).

$\text{CoMo}/\text{Al}_2\text{O}_3$  [2–4]. Commercial sulfided catalysts are deactivated due to sulfur removal from the catalysts composition and oxidation of the active sulfide phase is occurred. At the same time, addition of sulfur-containing agents ( $\text{H}_2\text{S}$ ,  $\text{CS}_2$ ) for maintaining of catalyst activity results to sulfur contamination of products. As an alternative for the sulfided catalysts mentioned above, non-sulfided systems based on transition metals (Ni, Cu, and Mo) were considered earlier [11–13]. The activity of unsulfided  $\text{NiMo}/\text{Al}_2\text{O}_3$  catalysts in the reduced form was also studied in the hydrodeoxygenation. In a reaction with a model compound (glacial acetic acid) a high activity was manifested by a reduced Mo-10Ni/ $\gamma$ - $\text{Al}_2\text{O}_3$  catalyst (33.2% conversion). After pyrolysis oil is treated in the presence of the same catalyst, its pH value rose from 2.16 to 2.84 and the hydrogen content increased from 6.61 to 6.93 wt%. Thus, it was shown that it is possible to improve the pyrolysis oil properties during hydrodeoxygenation and esterification of carboxyl groups of the compounds included in its composition [14]. The high content of organic acids in pyrolysis oil not only causes its corrosive properties, such as high corrosiveness and acidity, but also introduces a number of limitations to its application. The pyrolysis oil hydrodeoxygenation catalysts should possess a sufficient stability to an acidic environment. The formation of the nickel-molybdenum alloys results in increasing the corrosion and thermal stability of the material and improves its hydrogenation activity. Such alloys are used as heat- and acid-resistant construction materials [15]. Thus, it was mentioned that the activity of Raney nickel increased twice in the glucose hydrogenation while doping it with molybdenum [16]. The activity of molybdenum-doped  $\text{Ni-ZrO}_2$  catalysts was studied in the hydrodeoxygenation of octanoic acid. It was shown that the introduction of Mo improves the adsorption ability of hydrogen and the acid properties of the catalyst. In the case of the bimetallic catalyst 10Mo/Ni-ZrO<sub>2</sub>, the main product of the octanoic acid conversion was the C<sub>8</sub> alkane with a 77% yield, whereas, in the presence of Ni-ZrO<sub>2</sub>, the acid converted primarily to the C<sub>7</sub> alkane with a 70% yield. Thus, the introduction of molybdenum allows the hydrodeoxygenation process to be more profitable way in terms of conservation of the number of carbon atoms [17].

The simplest way to prepare such catalytic systems is the reduction of nickel molybdate, which is also a precursor of active structures in the sulfided form. Depending on the reduction conditions, the result is stable NiMo structures with different composition. Thus, Tsurov et al. [18] investigated the composition of the catalyst and its catalytic properties depending on the  $\alpha$ - $\text{NiMoO}_4$  reduction temperature. It was noted therein that the formation of a Ni-Mo alloy suppresses hydrogenation, but not hydrogenolysis.

In the present work we studied the activity and stability of Ni-Mo-containing catalysts in the hydrotreating of pyrolysis oil using anisole as a model compound. The catalysts are multicomponent systems resulting from the reduction of  $\text{NiMoO}_x\text{-SiO}_2$  sample in the temperature range of 300–750 °C (the sample is prepared by the sol-gel method, and its main component is  $\text{NiMoO}_4$ ). The reduction temperatures were determined according to the temperature-programmed reduction (TPR) data. To determine the composition of the active phase after reduction, these systems have been studied by X-ray diffraction (XRD) and X-ray photoelectron spectroscopy (XPS).

## 2. Experimental

### 2.1. Catalyst preparation

A sol-gel method was applied to synthesize  $\text{NiMoO}_x\text{-SiO}_2$ . To obtain a homogeneous system and to avoid the effect of nickel and molybdenum oxides on reduction processes, the ratio Ni/Mo = 1 was used. It allowed forming nickel molybdate as a pre-

**Table 1**  
The elemental composition of  $\text{NiMoO}_x\text{-SiO}_2$ .

Ni (wt%)	Mo (wt%)	$\text{SiO}_2$ (wt%)	Ni/Mo
28	43	2	1

cursor for active component. The 35 g of  $\text{NiCO}_3\cdot 3\text{Ni}(\text{OH})_2\cdot 2.7\text{H}_2\text{O}$  (Taurus, 98%) and 65 g  $(\text{NH}_4)_6\text{Mo}_7\text{O}_{24}\cdot 4\text{H}_2\text{O}$  (Laverna, 99%) were stirred with an 100 ml ammonia solution at room temperature. The amounts of the metal precursors were calculated to obtain a required Ni/Mo ratio—1:1. While stirring for 1 h the 2 ml ethylsilicate-32 was added to the suspension. The obtained precipitate was filtered, dried during 24 h and calcined at 500 °C for 1 h in air. The elemental composition of  $\text{NiMoO}_x\text{-SiO}_2$  is given in Table 1.

The  $\text{SiO}_2$  was used as a stabilizing agent, which has no activity in the hydrogenation process. Before the reaction the catalysts were activated by reduction with hydrogen; the reduction temperatures (300, 470, 570, and 750 °C) were determined from the TPR data.

### 2.2. Catalyst characterization

**Temperature programmed reduction.** Catalyst precursor  $\text{NiMoO}_x\text{-SiO}_2$  (0.1 g) was placed in a U-tube quartz reactor and treated in a reducing atmosphere (10 vol.% of  $\text{H}_2$  balanced in Ar at a flow rate of 20 ml/min) with a constant heating rate of approximately 4 °C/min up to 900 °C. The hydrogen concentration in the outlet stream during reduction was measured with a thermal conductivity detector.

The amount of  $\text{H}_2$  consumed in the runs was quantified by the peak-area integration method.  $\text{NiO}$ , which was prepared by calcination of  $\text{NiCO}_3\cdot 3\text{Ni}(\text{OH})_2\cdot 2.7\text{H}_2\text{O}$  (Taurus, 98%) for 2 h at 600 °C in air flow, was used to calibrate the TCD response.

**X-ray diffraction.** The phase composition of the spent catalysts was studied using a D8 X-ray diffractometer (Bruker, Germany) equipped with the Goebel mirror, generating a parallel X-ray beam of the  $\text{CuK}\alpha$  radiation ( $\lambda = 1.5418 \text{ \AA}$ ).

The chemical analysis of the catalyst surface was performed using X-ray photoelectron spectroscopy. The XPS measurements were performed on a SPECS's Surface Nano Analysis GmbH (Germany) photoelectron spectrometer equipped with a PHOIBOS-150-MCD-9 hemispherical electron energy analyzer, a FOCUS-500 X-ray monochromator, and an XR-50M X-ray source with a double Al/Ag anode. The spectrometer was also equipped with a high-pressure cell (HPC) which enables to heat samples before analyzing in gaseous mixtures at pressures up to 0.5 MPa. The core-level spectra were obtained using the monochromatic  $\text{AlK}\alpha$  radiation ( $h\nu = 1486.74 \text{ eV}$ ) and fixed analyzer pass energy of 20 eV under ultrahigh vacuum conditions. The charge correction was performed by setting the  $\text{Ni}2p_{3/2}$  peak at 852.7 eV corresponding to nickel in the metallic state. Such correction is justified at least for reduced catalysts with high content of metals [12]. The C1s binding energy of adventitious carbon surface impurities changed between 284.3 and 284.4 eV that confirmed the suitability of our approach. Relative element concentrations were determined from the integral intensities of XPS peaks using the cross-sections according to Scofield [19]. For detailed analysis the spectra were fitted into several peaks after the background subtraction by the Shirley method. The fitted procedure was performed using the CasaXPS software. The line shapes were approximated by the convolution of Gaussian and Lorentz functions. Before the XPS analysis, the catalysts were additionally reduced in 1 bar  $\text{H}_2$  at 300 and 400 °C for 30 min in the HPC.

The metallic surface area of the reduced samples was determined by **CO pulse chemisorption measurements** using a Chemosorb analyzer ("Modern laboratory equipment", Russia). CO uptakes were measured at 25 °C after prereduction at 350 °C. A sto-

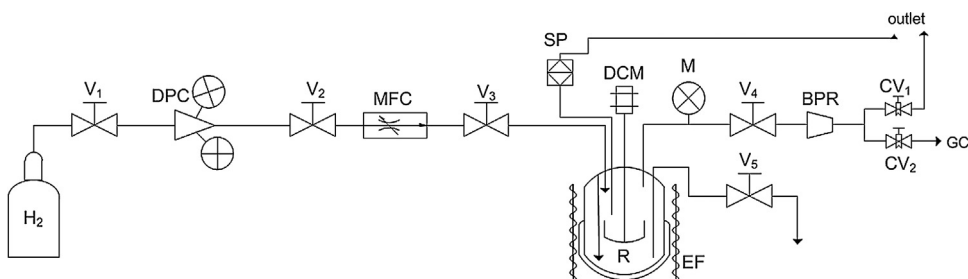


**Fig. 1.** Set-up scheme: V<sub>1</sub>–V<sub>5</sub>—valves; DPC—downstream pressure controller; MFC—mass flow controller; SP—safety pressure rupture disk; DCM—DC Motor; R—reactor; EF—electric furnace; M—manometer; BPR—back pressure regulator; CV<sub>1</sub> and CV<sub>2</sub>—control valves.

ichiometry of M:CO = 1:1 was assumed, where M was active site [20–22]

The specific surface area ( $S_{co}$ ) and average particle size ( $d$ ) were calculated as follows:

$$S_{co} \left( \frac{m^2}{g} \right) = \frac{V}{22414} N_{Av} \times \frac{n \times a_m}{m} \times \frac{100}{w}$$

$$d = 6 \left( \frac{V_m \times m \times \times}{100 \times M \times a_m \times V \times n} \right)$$

where  $N_{Av}$  is Avogadro's number ( $6.022 \times 10^{23}$ );  $V$  is the adsorbate volume required to form a monolayer coating ( $\text{cm}^3$ );  $n$  is the stoichiometric factor of CO adsorption;  $m$  is the sample mass (g);  $a_m$  is the surface area occupied by the surface atoms ( $\text{m}^2$ );  $w$  is the metal mass fraction (%);  $M$  is the atomic mass of metal (g/mol);  $V_m$  is the volume occupied by the metal atom ( $\text{m}^3$ ).

### 2.3. Experimental setup

Catalytic hydrotreatment of anisole was carried out in a high-pressure setup (Autoclave Engineers, USA) in a sealed 300-ml stainless steel batch reactor (EZE Seal type). The reactor was equipped with a magnetic stirrer, a thermocouple, a pressure sensor, and a system for controlling stirring rate, temperature, and pressure (Fig. 1). Before the reaction, the catalysts (1 g of a fine powder) were activated directly in the reactor by the reduction in a flow of 100% H<sub>2</sub> (100 ml/min) for 1 h at 350 °C and 0.1 MPa. After the activation, 100 ml of 15 wt% anisole (ACROS Organics, 99%) in undecane (Sigma-Aldrich, 99%) was placed into the reactor at 0.1 MPa and 25 °C without access of air to prevent the catalyst oxidation. The reactions of anisole were carried out under isothermal conditions (300 °C) and a total pressure of 6 MPa. The hydrogen pressure was kept at the same level in the all experiments. The reaction conditions were selected in terms of the required hydrogen excess to provide the first-order kinetics with respect to the organic reagents. During the reaction, liquid products were taken at certain intervals and analyzed. The stirring rate was 2000 rpm, the catalysts were used in the form of fine powder, the reaction was carried out in a tenfold excess of hydrogen with respect to anisole.

### 2.4. Product analysis

Qualitative analysis of liquid products of the hydrodeoxygenation and hydrogenation of anisole was carried out using a Varian Saturn 2000 GC/MS spectrometer equipped with an ion trap and an HP-5 quartz capillary column (stationary phase: 5% phenyl–95% dimethylpolysiloxane, column length 30 m, inner diameter 0.25 mm). Quantitative analysis of the liquid products was performed using a Hromos GC 1000 chromatograph equipped with a Zebron ZB-35HT capillary column (stationary phase: 35% phenyl–65% dimethylpolysiloxane, 30 m × 0.32 mm × 0.25 μm). The injector and detector temperatures were 280 and 260 °C,

respectively. The following temperature program was used for analysis: 70 °C hold for 10 min, 15 °C/min for 4 min, 280 °C hold for 6 min. A 0.3 μl sample was injected into the GC/MS spectrometer with a chromatographic syringe; argon was used as a carrier gas. The reaction mixture components were identified by retention times on the chromatogram, which were determined separately for each component in the calibration process. The internal normalization was used for the quantitative calculation of the component concentrations in the mixture.

The deoxygenation selectivity (HDO) was calculated as follows:

$$\text{HDO}(\%) = \frac{n_{\text{anisole}}^0 \times X - \sum_i n_i \times a_i}{n_{\text{anisole}}^0 \times X} \times 100 = \left( 1 - \frac{\sum_i n_i \times a_i}{n_{\text{anisole}}^0 \times X} \right) \times 100$$

$$X(\%) = \frac{n_{\text{anisole}}^0 - n_{\text{anisole}}^{\text{final}}}{n_{\text{anisole}}^0} \times 100$$

where  $n_{\text{anisole}}^0$  is the initial amount of anisole (mol),  $n_{\text{anisole}}^{\text{final}}$  is the final amount of anisole (mol),  $n_i$  is the amount of  $i$ -product (mol) in the liquid phase (except for unreacted anisole), and  $a_i$  is the number of oxygen atoms in the molecule of  $i$ -product.

### 2.5. Corrosion resistance test

The catalysts resistance to corrosion in acidic medium was determined by the treatment with glacial acetic acid. The catalysts in the reduced form (1 g) were treated in glacial acetic acid (100 ml) at 118 °C for 2 h, and then the samples were separated from the solution. The corrosion resistance was calculated from the Ni and Mo concentrations in the solution and the samples mass loss (wt%) after the acidic treatment.

## 3. Results and discussion

### 3.1. Catalyst characterization results

Temperature programmed reduction technique was applied to study the reduction behavior of the oxide precursor NiMoO<sub>x</sub>–SiO<sub>2</sub>. The TRP profile is presented in Fig. 2. Reduction of α-NiMoO<sub>4</sub> was widely discussed in the literature, but there is no consensus about the sequence of phase transformations and the intermediate state composition. According to different authors, at the first step 300–600 °C NiMoO<sub>4</sub> reduced to Ni and MoO<sub>2</sub> [23]. Ni, MoO<sub>2</sub>, Ni<sub>4</sub>Mo [24], Ni and Mo<sub>2</sub>O<sub>3</sub>, NiMo alloy and MoO<sub>2</sub> [18,25] or to the mixed

oxide– $\text{NiMoO}_x$  [26]. The second stage occurs in a temperature range of 600–800 °C and results in the formation of various metallic compounds: Mo, NiMo alloys, intermetallics  $\text{Ni}_3\text{Mo}$ ,  $\text{Ni}_4\text{Mo}$  [24,26]. The TPR profile also can have various positions of the peaks in different experiments, it depends on the heating rate, crystallite size, crystallite size, etc [27]. Madeira et al [24] and Brito et al. [27] got a similar TPR profile, which had two maxima at about 575 and 730 °C. The TPR profile of the calcined sample on Fig. 2 consists of a narrow peak at 450 °C and two broad peaks at 570 and 750 °C. The hydrogen consumption begins at 400 °C and has maximum at 450 °C. According to this picture, this peak may be assigned to the  $\text{Ni}^{2+}$  reduction [28]. In works [27,29] no peak at 450 °C was detected, however the small shoulder at 320–400 °C, which then transform to the broad peak at 520–550 °C, was observed. A clear shape of this peak in our case might indicate also the reduction of  $\text{Mo}^{6+}$  to the metallic state, and the transition of  $\text{Mo}^{6+}$  to  $\text{Mo}^{4+}$ . Probably, the major part of the process takes place at a temperature of 570 °C. It is worth considering that reduced metallic nickel could activate the hydrogen molecule, which promoted the reduction of  $\text{Mo}^{6+}$  [27]. According to [29] the peak at 575 °C belongs to the reduction of  $\text{Mo}^{6+}$  to  $\alpha$ - $\text{NiMoO}_4$  while in the case of  $\beta$ - $\text{NiMoO}_4$  that peak shifts to the higher temperature (635 °C). When the reduction performed up to 680 °C, the third peaks appeared. Reduction of residual forms of molybdenum oxide passes at 750 °C. Additionally, the ratios of the first to the second signals are larger ( $S_{570}/S_{750} = 2.3$ ), suggesting that more molybdenum is reduced in the first step. Because the sample could

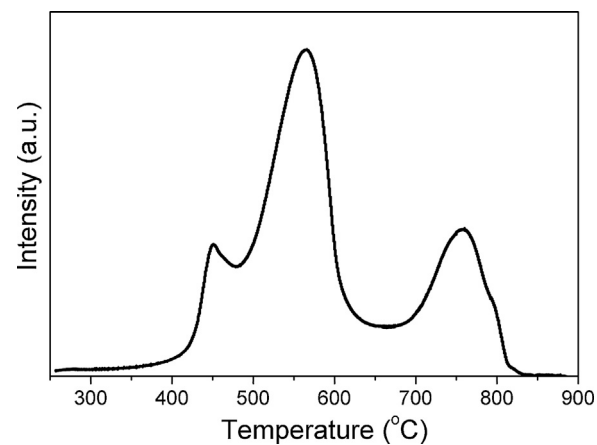


Fig. 2.  $\text{H}_2$ -TPR profile of catalyst precursor  $\text{NiMoO}_x\text{-SiO}_2$ .

be not homogeneous it could contain individual molybdenum oxide particles, so the main TPR profile is a superposition of  $\text{NiMoO}_4$  and  $\text{MoO}_3/\text{MoO}_2$  profile. That is why there is a shoulder around 800 °C.

The reduction temperatures 470, 570 and 750 °C were chosen according to the results of TPR experiments: the TPR profile exhibits maxima near these temperatures. Therefore, it was reasonable to test the composition of the Ni–Mo–O system after reduction namely

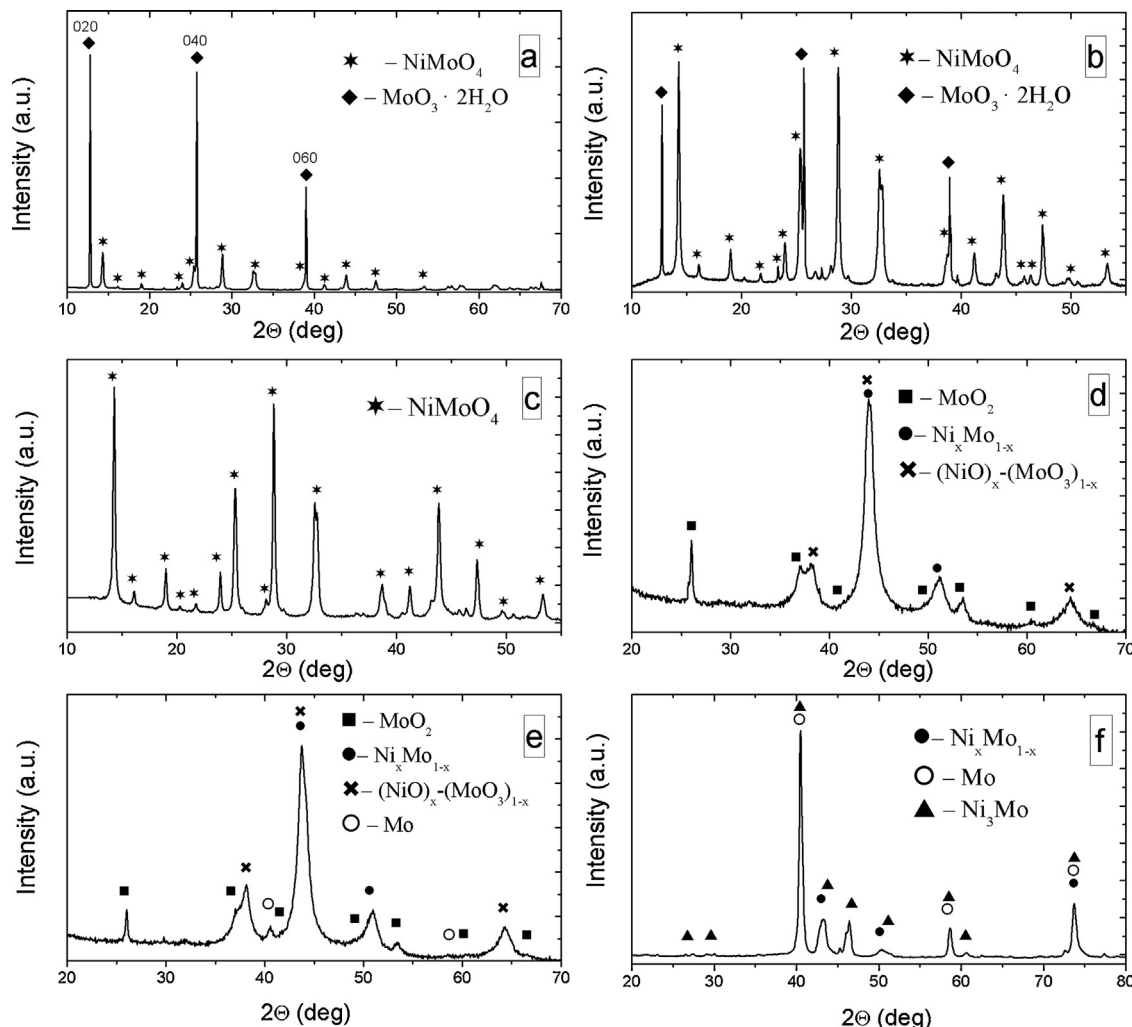


Fig. 3. XRD patterns of catalysts:  $\text{NiMoO}_x\text{-SiO}_2$  (a, b), 300– $\text{NiMo-SiO}_2$  (c), 470– $\text{NiMo-SiO}_2$  (d), 570– $\text{NiMo-SiO}_2$  (e), 750– $\text{NiMo-SiO}_2$  (f).

at these temperatures, to elucidate the mechanism of the reduction of such systems. The reduction of  $\text{NiMoO}_4$  at these temperatures results in the formation of different Ni- and Mo-containing phases. Subsequently, catalytic activity tests were performed to understand the effect of these phases.

In order to identify the reduction products XRD analysis was performed after the reduction at selected temperatures corresponding to the maxima in the TPR profile and 300 °C. Fig. 3 shows the XRD patterns of the non-reduced catalyst  $\text{NiMoO}_4\text{-SiO}_2$  (a, b) and the same catalyst activated in  $\text{H}_2$  at 300 (c), 470 (d), 570 (e), and 750 (f) °C.

The XRD patterns of the  $\text{NiMoO}_4\text{-SiO}_2$  catalyst in the oxidized state were recorded when the sample was fixed (3a) and when it rotated at 15 rpm (3b). In those experiments, the only differences could be found in the relative intensity of the three reflections (interplanar distances  $d = 6.92, 3.47, 2.31 \text{ \AA}$ ) belonging to the phase  $\text{MoO}_3\cdot2\text{H}_2\text{O}$  (JCPDS card No. 01-07-01513). Their varying intensity, with and without rotation, indicates that the sample contains few big grains of  $\text{MoO}_3\cdot2\text{H}_2\text{O}$  textured in the [0k0] direction. Hereby the sample contains a few big grains of textured  $\text{MoO}_3\cdot2\text{H}_2\text{O}$  and non-textured oxide  $\text{MoO}_3\cdot2\text{H}_2\text{O}$ . At a certain orientation of the sample, large textured  $\text{MoO}_3\cdot2\text{H}_2\text{O}$  particles make a big contribution to the diffraction pattern (Fig. 3a). Rotation leads to a better averaging (a larger sample volume). So the contribution of a small amount of big grains of textured  $\text{MoO}_3\cdot2\text{H}_2\text{O}$  reduces. As a result the intensity of the corresponding reflections of  $\text{MoO}_3\cdot2\text{H}_2\text{O}$  decreases. Moreover, the diffraction pattern contains peaks corresponding to the  $\text{NiMoO}_4$  phase (JCPDS card No. 330948). The analysis of the sample reduced at 300 °C showed that the sample contains only the nickel molybdate phase, while the  $\text{MoO}_3\cdot2\text{H}_2\text{O}$  phase is absent (Fig. 3c). This is most likely due to the fact that the water evaporates and the crystalline destructs during heating.

The XRD patterns of the catalyst reduced at 470 °C (Fig. 3d) contains the reflections of  $\text{MoO}_2$ , however the position of the other peaks is very different from the original angle values. The reduced catalyst contains a  $\text{Ni}_x\text{Mo}_{1-x}$  metallic solid solution of Ni modified by molybdenum ions. The composition of Ni-Mo solid solutions was estimated by the linear dependence of the unit cell parameter of the known compounds: Mo (JCPDS card No. 421120), Ni (JCPDS card No. 040850),  $\text{Mo}_{0.09}\text{Ni}_{0.91}$  (JCPDS card No. 105048),  $\text{Mo}_{0.36}\text{Ni}_{0.64}$  (JCPDS card No. 105045), and  $\text{Mo}_{0.984}\text{Ni}_{0.016}$  (JCPDS card No. 105049) on the content of “ $x$ ” in  $\text{Ni}_x\text{Mo}_{1-x}$  (Fig. 4). The unit cell parameter (3.575 Å) can be used to determine the composition of the solid solution, which corresponds to  $\text{Ni}_{0.88}\text{Mo}_{0.12}$ . The other peaks can be attributed to the Ni-Mo-oxide phase with a NiO-type structure whose reflections are displaced toward distant angles with respect to NiO. The composition of this phase is still not completely determined. Thus, the study of the  $\text{NiMoO}_4$  reduc-

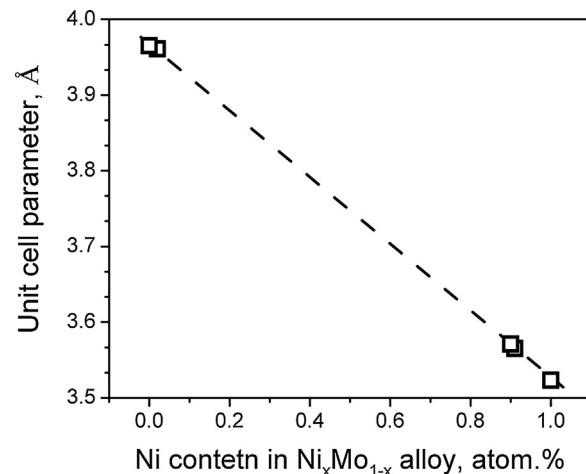


Fig. 4. Unit cell parameter as a function of Ni-Mo alloy composition.

tion led many authors to conclude that there are different kinds of intermediates that in the most cases correspond to the composition of  $\text{NiMoO}_x$  or  $\text{Ni}_2\text{Mo}_3\text{O}_8$  [30]. For instant, Rodrigues et al. [31] suggested that the intermediate is a mixture of  $\text{Ni}_4\text{Mo}$ , Ni, and  $\text{NiO}$ .

Moreover, in addition to the reflections of  $\text{MoO}_2$ ,  $\text{NiMoO}_y$ , and  $\text{Ni}_x\text{Mo}_{1-x}$ , the XRD pattern of the catalyst reduced at 570 °C showed the peaks of molybdenum in the metallic state (Fig. 3e). In this case, the metallic solution has the composition  $\text{Ni}_{0.84}\text{Mo}_{0.16}$ , and its lattice parameter is 3.595 Å. Reduction of the catalyst at 750 °C leads to the formation of Mo,  $\text{Ni}_3\text{Mo}$ , and  $\text{Ni}_x\text{Mo}_{1-x}$  (Fig. 3f). The lattice parameter of  $\text{Ni}_x\text{Mo}_{1-x}$  is 3.618 Å, which corresponds to the composition  $\text{Ni}_{0.79}\text{Mo}_{0.21}$  of the solid solution. Table 2 shows the overall phase composition data for all samples under the study.

Fig. 5 shows the proposed scheme of the catalyst reduction. The first stage consists of heating to 300 °C, which leads to the decomposition of the crystalline hydrate and the formation of an amorphous molybdenum oxide. When nickel molybdate is reduced in hydrogen at 470 °C,  $\text{NiMoO}_4$  converts to a  $\text{NiMoO}_x$  oxide with the NiO-type structure and the formation of  $\text{MoO}_2$  and the  $\text{Ni}_x\text{Mo}_{1-x}$  solid solution. In this case,  $\text{Ni}^{2+}$  reduced to a metallic nickel activates  $\text{H}_2$  and contributes to the reduction of  $\text{Mo}^{6+}$  to  $\text{Mo}^{4+}$  ( $\text{MoO}_2$ ) [32] with a subsequent formation of an alloy. Upon activation of the catalyst at 570 °C,  $\text{MoO}_2$  is partially reduced to molybdenum in the metallic state. At the final stage corresponding to the reduction temperature of 750 °C, the alloy is partially reduced to  $\text{Ni}_3\text{Mo}$  and  $\text{MoO}_2$  is completely reduced. The formation of  $\text{Ni}_3\text{Mo}$  may occur from  $\text{Ni}_x\text{Mo}_{1-x}$  alloy or NiO-type particles. To determine the formation way we decided to carry out the additional XRD study of sample

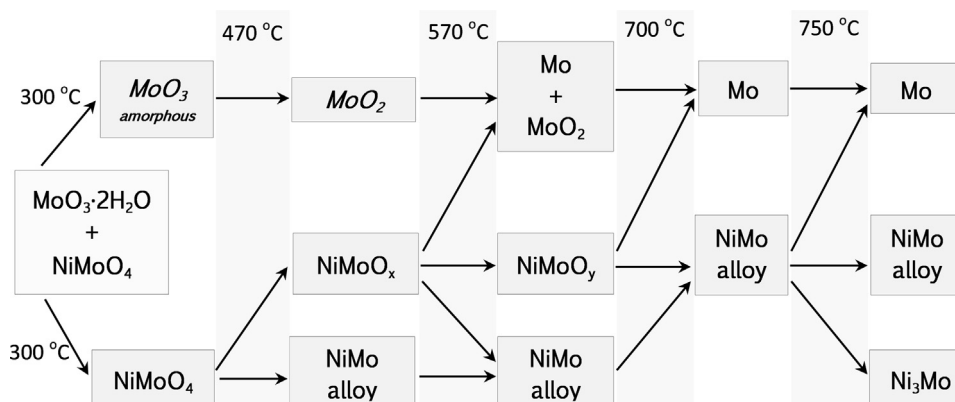
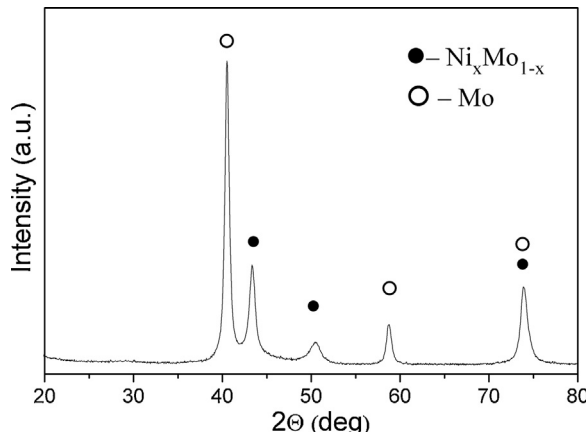


Fig. 5. Catalyst reduction scheme. The crystalline hydrate reduction is shown in italic.

**Table 2**

The phase composition of the catalyst.

Catalyst	NiMoO <sub>x</sub> -SiO <sub>2</sub>	300-NiMo-SiO <sub>2</sub>	470-NiMo-SiO <sub>2</sub>	570-NiMo-SiO <sub>2</sub>	750-NiMo-SiO <sub>2</sub>
The phase composition	NiMoO <sub>4</sub> MoO <sub>3</sub> ·2H <sub>2</sub> O	NiMoO <sub>4</sub>	Mo <sub>2</sub> , NiMoO <sub>x</sub> Ni <sub>0.88</sub> Mo <sub>0.12</sub>	Mo <sub>2</sub> , NiMoO <sub>y</sub> Ni <sub>0.84</sub> Mo <sub>0.16</sub> Mo	Mo Ni <sub>0.79</sub> Mo <sub>0.21</sub> Ni <sub>3</sub> Mo

**Fig. 6.** XRD patterns of catalysts NiMoO<sub>x</sub>-SiO<sub>2</sub> reduction at 700 °C.

reduced at 700 °C (Fig. 6). According to the data obtained the heating of sample at 700 °C causes to formation of two metallic phases: significant amount of Mo and the Ni<sub>0.81</sub>Mo<sub>0.19</sub> solid solution. The content of Mo<sup>o</sup> and MoO<sub>2</sub> at 570 °C is very small and it cannot give enough quantity of molybdenum at 700 °C. Also the sequence of formation Ni<sub>0.88</sub>Mo<sub>0.12</sub>–Ni<sub>0.84</sub>Mo<sub>0.16</sub>–Ni<sub>0.81</sub>Mo<sub>0.19</sub> requires increasing of molybdenum content. These facts suggest that the molybdenum can be formed from the NiMoO<sub>x</sub> structure. In addition, the XRD data at 700 °C shows that Ni<sub>3</sub>Mo is produced from the Ni<sub>x</sub>Mo<sub>1-x</sub> alloy.

The XRD results are consistent with TPR data. The amount of H<sub>2</sub> consumed in the TPR runs indicates that the oxide form of catalysts is completely reduced to the metallic state. Indeed, TPR data for the NiMoO<sub>x</sub>-SiO<sub>2</sub> sample (see Table 3) show that the total H<sub>2</sub> consumption is 17.6 mmol/g, which is close to the calculated value 17.9 mmol/g required to reduce the total amount of NiMoO<sub>4</sub> in the sample. The small amount of amorphous MoO<sub>3</sub> was not taken into account during the calculation. The reduction of the catalyst at 450 °C resulted in a H<sub>2</sub> uptake of 1.5 mmol/g, which is equivalent to the reduction of less than 30% of nickel assuming, 1) the stoichiometry for the direct reduction of Ni<sup>2+</sup> to Ni<sup>o</sup> and 2) the reduction of molybdenum with the formation of an alloy Ni<sub>0.88</sub>Mo<sub>0.12</sub>. This indicates that most of nickel is reduced at higher temperatures. The reduction of the catalyst at 570 °C resulted in the H<sub>2</sub> consumption of 11.3 mmol/g, which is sufficient for the partial reduction of Ni<sup>2+</sup>, Mo<sup>6+</sup> and Mo<sup>4+</sup>. According to the XRD, nickel at this temperature is not completely reduced, which can be due to strong interaction of Ni with Mo in NiO-type structures. Besides, the content of Mo<sup>o</sup> and MoO<sub>2</sub> at 570 °C is very small while the Ni content in the NiMo alloy is very high. Thus, the amount of NiO in NiMoO<sub>x</sub> is very low. It can be assumed that the TPR peak at 750 °C corresponds mostly to the reduction of molybdenum oxide. For the complete reduction of molybdenum from Mo<sup>4+</sup> to Mo<sup>o</sup> in the sample NiMoO<sub>4</sub>-SiO<sub>2</sub>, the necessary consumption of H<sub>2</sub> would be 9.1 mmol/g. Therefore, the H<sub>2</sub> uptake of 4.8 mmol/g, which was observed in the third peak, is equivalent to the reduction of 52% of Mo<sup>4+</sup> to Mo<sup>o</sup>.

To study the chemical composition of the near-surface layer, the samples were investigated by XPS. Before recording spectra, the samples were pre-reduced directly in the high-pressure cell of the spectrometer in hydrogen at 300 °C. The relative atomic concentrations of the detected elements determined on the basis of

the XPS data are shown in Table 4. As can be seen, the atomic ratio of Ni/Mo for the catalysts increases along with the temperature of pre-treatment in hydrogen, which can be associated with the nickel segregation to the surface. It also shows that molybdenum is in the oxide form on the surface at a temperature of 300 °C, and it is mainly in the metallic state at 750 °C.

Fig. 7 shows the Ni2p and Mo3d spectra of the catalysts. The shape of Ni2p spectra indicates that nickel in the catalysts is in the metallic state. Indeed, the Ni2p spectra contain two sharp Ni2p<sub>3/2</sub> and Ni2p<sub>1/2</sub> peaks at 852.7 and 869.9 eV, which correspond to nickel in the metallic state. This is also indicated by the shape of the Ni2p spectra and by the value of the spin-orbit splitting (difference in the Ni2p<sub>1/2</sub> and Ni2p<sub>3/2</sub> binding energies) equal to 17.2 eV (Table 5). For nickel in the oxidized state Ni<sup>2+</sup>, this value is 17.6–17.8 eV [35–38]. Moreover, the Ni<sup>2+</sup> compounds have the higher Ni2p<sub>3/2</sub> binding energies and shake-up satellites, which are ~6 eV higher on the binding energy scale from the main peak. The presence of these satellites determined by multielectron processes [34–36] is characteristic only for Ni<sup>2+</sup> compounds. For example, the intense shake-up satellites are observed in the spectra of NiO, Ni(OH)<sub>2</sub>, NiSiO<sub>3</sub>, etc. [39–41]. At the same time, the spectra of metallic nickel and of Ni<sup>3+</sup> compounds do not have these satellites [33,42]. The decomposition of the spectra into individual components indicates that nickel is completely reduced to the metallic state.

In the 470-NiMo-SiO<sub>2</sub> catalyst, molybdenum is partly reduced to the metallic state. When reduction is carried out at 750 °C, molybdenum is reduced completely. Thus, we observe the single Mo3d<sub>5/2</sub>-Mo3d<sub>3/2</sub> doublet in its spectra with the binding energy of Mo3d<sub>5/2</sub> equal to 227.4 eV, which corresponds to molybdenum in the metallic state, for which the Mo3d<sub>5/2</sub> binding energies are given in the literature in the range 227.7–227.9 eV [43–45]. The value 227.4 is different from the literature data; it is due to the chemical shift of Mo3d<sub>5/2</sub> peak.

In the Mo3d spectrum of the catalyst 470-NiMo-SiO<sub>2</sub>, we observe two doublets Mo3d<sub>5/2</sub>-Mo3d<sub>3/2</sub> with the Mo3d<sub>5/2</sub> binding energies equal to 227.8 and 229.6 eV. The first doublet can be attributed to molybdenum in the metallic state, and the second one—to molybdenum in the Mo<sup>4+</sup> state. The Mo3d<sub>5/2</sub> binding energies of Mo<sup>4+</sup>, Mo<sup>5+</sup>, and Mo<sup>6+</sup> are given in the literature varies in the ranges of 229.2–229.9, 230.8–231.6, and 232.7–233.2 eV, respectively [43–47]. There are two Mo3d<sub>5/2</sub>-Mo3d<sub>3/2</sub> doublets observed for the catalyst 300-NiMo-SiO<sub>2</sub> with the Mo3d<sub>5/2</sub> binding energies equal to 229.0 and 231.3 eV. These values correspond to molybdenum in the Mo<sup>4+</sup> and Mo<sup>5+</sup> states, respectively.

### 3.2. Catalytic activity of NiMoO<sub>x</sub>-SiO<sub>2</sub> in anisole hydrotreatment

The main product obtained during the hydrotreatment of anisole is cyclohexane; the intermediate components are methoxycyclohexane, cyclohexanol, benzene, and methylanisoles. According to mass-spectrometric data, unidentified products that may appear because of polymerization or other side reactions were not formed. According to the results of the composition of liquid products after the reaction, we proposed an anisole conversion scheme that includes three reaction pathways (Fig. 8). The first reaction pathway is for the hydrodeoxygenation of anisole with a cleavage C<sub>ar</sub>—O bound and the formation of benzene, which then converts to cyclohexane. The second pathway is meant for the

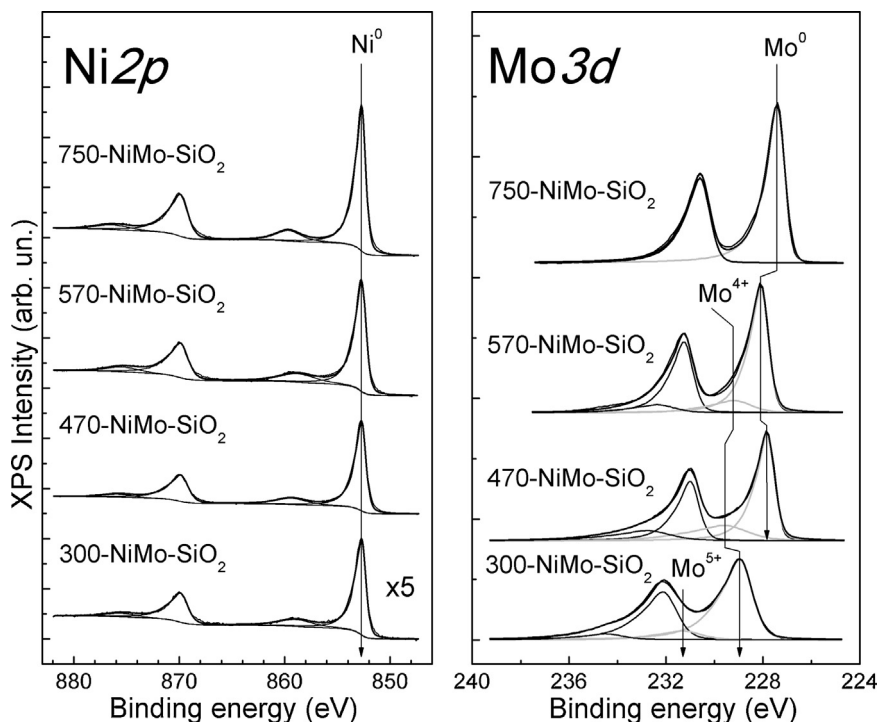
**Table 3**TPR data of NiMoO<sub>4</sub>-SiO<sub>2</sub> samples.

Peak	T <sub>onset</sub> <sup>a</sup> (°C)	T <sub>max</sub> <sup>b</sup> (°C)	T <sub>term</sub> <sup>c</sup> (°C)	H <sub>2</sub> consumption (mmol/g <sub>cat</sub> )
1st peak	350	450	480	1.5
2nd peak	480	570	665	11.3
3rd peak	670	750	840	4.8
Total H <sub>2</sub> consumption (mmol/g <sub>cat</sub> )				17.6

<sup>a</sup> Temperature of the onset of a reduction peak.<sup>b</sup> Temperature of the peak maximum.<sup>c</sup> Temperature of termination of a reduction peak.**Table 4**

The relative elements concentrations in the surface layer of the investigated catalysts.

Catalyst	[Ni]/[Mo]	[Ni <sup>0</sup> ]/[Ni <sub>ali</sub> ] (%)	[Mo <sup>0</sup> ] <sup>a</sup> /[Mo <sub>ali</sub> ] (%)	[Si]/[Mo]
300-NiMo-SiO <sub>2</sub>	0.08	100	0	–
470-NiMo-SiO <sub>2</sub>	0.38	100	68	0.35
570-NiMo-SiO <sub>2</sub>	0.39	100	81	0.66
750-NiMo-SiO <sub>2</sub>	0.57	100	100	0.57

<sup>a</sup> The peak position in the region 227.5–227.8 eV, corresponding molybdenum in the metallic state.**Fig. 7.** The Ni2p and Mo3d spectra of the catalysts studied. The Ni2p spectra are normalized to the integral intensity of the corresponding Mo3d spectra.**Table 5**The of Mo3d<sub>5/2</sub>, Ni2p<sub>3/2</sub>, and O1s binding energies (eV) determed for the catalysts.

Catalyst	Mo3d <sub>5/2</sub> (ox.)	Mo3d <sub>5/2</sub> (metal.)	Ni2p <sub>3/2</sub>	ΔNi2p <sup>a</sup>	O1s
300-NiMo-SiO <sub>2</sub>	229.0 231.3	–	852.7	17.2	530.1 531.0 532.1
470-NiMo-SiO <sub>2</sub>	229.6	227.8	852.70	17.2	530.2 532.7
570-NiMo-SiO <sub>2</sub>	229.2	228.1	852.7	17.2	530.5 532.8
750-NiMo-SiO <sub>2</sub>	–	227.4	852.7	17.2	530.1 532.9
NiO <sup>b</sup>	–	–	853.8	17.7	529.5 531.6
Ni <sup>c</sup>	–	–	852.7	17.2	–

<sup>a</sup> The value of the spin-orbit splitting equal to the difference in the Ni2p<sub>1/2</sub> and Ni2p<sub>3/2</sub> binding energies.<sup>b</sup> Nickel oxide previously obtained by oxidizing a nickel foil in oxygen directly in HPC of the spectrometer.<sup>c</sup> Pre-cleaned nickel foil (Ni 99.99%).

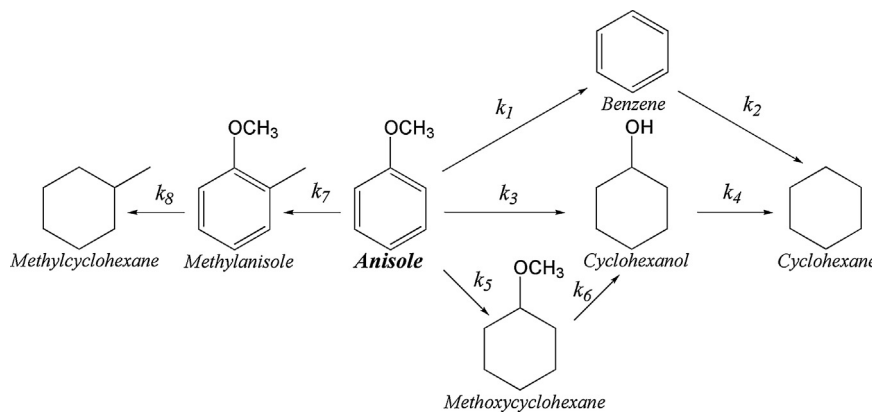


Fig. 8. The proposed scheme of anisole conversion pathways ( $k_i$  is the first-order rate constants).

hydrogenation of the aromatic ring of anisole with the formation of methoxycyclohexane. The third pathway includes an additional reaction of methyl substitution of anisole in the benzene ring with subsequent processes of hydrogenation and hydrodeoxygenation of methylanisoles obtained. The third pathway includes an additional reaction of methyl substitution of anisole in the benzene ring with subsequent processes of hydrogenation and hydrodeoxygenation of methylanisoles obtained. In this case, there is a possibility of reverse demethylation. Thus, Odebunmi and Ollis [48] studied the hydrodeoxygenation of m-, o-, and p-cresols on CoO-MoO<sub>3</sub>/γ-Al<sub>2</sub>O<sub>3</sub> sulfided catalysts, in which case the main product was methylcyclohexane.

The kinetic modeling was based on the proposed scheme of reactions, and calculations were carried out with the use of the following model:

$$\frac{dC_i}{dt} = R_i, R_i = \sum_m r_m, r_m = k_m C_m^n, \text{ where } k_m \text{ is the rate constant,}$$

$C_i$  and  $C_m$  are the mole fractions of each component,  $R_i$  is the reaction rate,  $n$  is the order of the reaction ( $n=1$  for all reactions except the reaction of the formation of methylanisole from anisole, where  $n=2$ ). An experimental point serves as  $t=0$ , are equal to the mole fractions of the corresponding compounds at the first point.

The system of equations was solved by the numerical integration using the Runge-Kutta method, and the kinetic parameters were found by the minimization of the sum of squared differences of the estimated and experimental values of the mole fraction of each compound for each experimental point. The minimizing function has the form:

$$F = \sum_i \sum_j \left( \frac{C_{ij\text{exp}} - C_{ij\text{calc}}}{C_{ij\text{exp}}} \right)^2$$

where  $j$  is the number of the experimental point;

$i$  is the serial number of the compound from the reaction scheme (anisole, benzene, cyclohexane, cyclohexanol, methylcyclohexane, methoxycyclohexane, and methylanisole). The concentration variations of the species in the reaction mixture as a function of reaction time and kinetic modeling results are shown in Fig. 9.

Fig. 9 shows that the concentration of transitional products for each sample does not exceed 8 mol%, which indicates a high hydrogenating activity of catalysts under these conditions, and that leads to a high yield of the final product (cyclohexane). The studies have shown that an increase in the reduction temperature reduces the yield of byproducts formed during the methylation of anisole (methylcyclohexane and methylanisole) and reached with the use of the 750-NiMo-SiO<sub>2</sub> catalyst.

Table 6 presents the estimated values of the constants of the reaction rates of anisole conversion. It follows from the values of

$k_1$  that an increase of the catalyst reduction temperature lowers the contribution of the HDO pathway. For the 750-NiMo-SiO<sub>2</sub> catalyst, the reaction rate constant along the pathway of methylanisole formation equals zero, though methylanisoles were found in their composition during the analysis of the reaction products. This is due to the fact that, during the heating of the reaction medium in the absence of hydrogen, the methylation of anisole also takes place. For the 470-NiMo-SiO<sub>2</sub> and 570-NiMo-SiO<sub>2</sub> catalysts, the formation of methyl-substituted products occurs at a higher rate with the subsequent formation of methylcyclohexane, which indicates that these catalysts are easier to methylate as compared to the sample reduced at 750 °C.

To determine the specific activity of the catalysts, we studied their metal surface by the CO chemisorption method. The results are presented in Table 7. The HDO pathway corresponds to the hydrogenolysis of the C<sub>ar</sub>—O bond in the anisole molecule without hydrogenation of the aromatic ring. The HYD pathway corresponds to the hydrogenation of the aromatic ring in anisole without oxygen removal.

The average particle size increases with an increase in the reduction temperature, which is caused by the sintering of the particles during reduction. There is no certain dependence of the specific activity on the reduction temperature. For example, the activity of the sample 570-NiMo-SiO<sub>2</sub> is lower than that of the sample 470-NiMo-SiO<sub>2</sub>. At the same time, the specific catalytic activity of the sample reduced at 750 °C exceeds several times the specific activity of the other catalysts. This is true for the specific activity in both HDO and HYD. The high specific activity of the sample 750-NiMo-SiO<sub>2</sub> may be due to the nature of its active component: all metallic particles in this catalyst are in the reduced state. Thus, the complete reduction of nickel to the metallic state leads to a higher activation of molecular hydrogen on the catalyst surface, which causes the high specific activity in the hydrogenation of anisole. At the same time, in the samples reduced at 470 and 570 °C, nickel is respectively in the form of alloys Ni<sub>0.88</sub>Mo<sub>0.12</sub> and Ni<sub>0.84</sub>Mo<sub>0.16</sub>. Its content in the composition of the alloy decreases, resulting in a slight decrease in the specific activity.

In contrast, the effective activity, which is defined via unnormalized constants  $k_i$ , was the higher, the lower was the reduction temperature. The activity decreases with an increase in the particle size, but this dependence is nonlinear. For example, for the samples 570-NiMo-SiO<sub>2</sub> and 750-NiMo-SiO<sub>2</sub>, the 12-fold increase in the particle size leads to the 2-fold decrease in the activity, while for the samples 470-NiMo-SiO<sub>2</sub> and 570-NiMo-SiO<sub>2</sub>, an increase in the particle size as low as 1.2-fold leads to the 1.6-fold decrease in the activity. Thus, the particle size is not the main reason for the activity decrease.

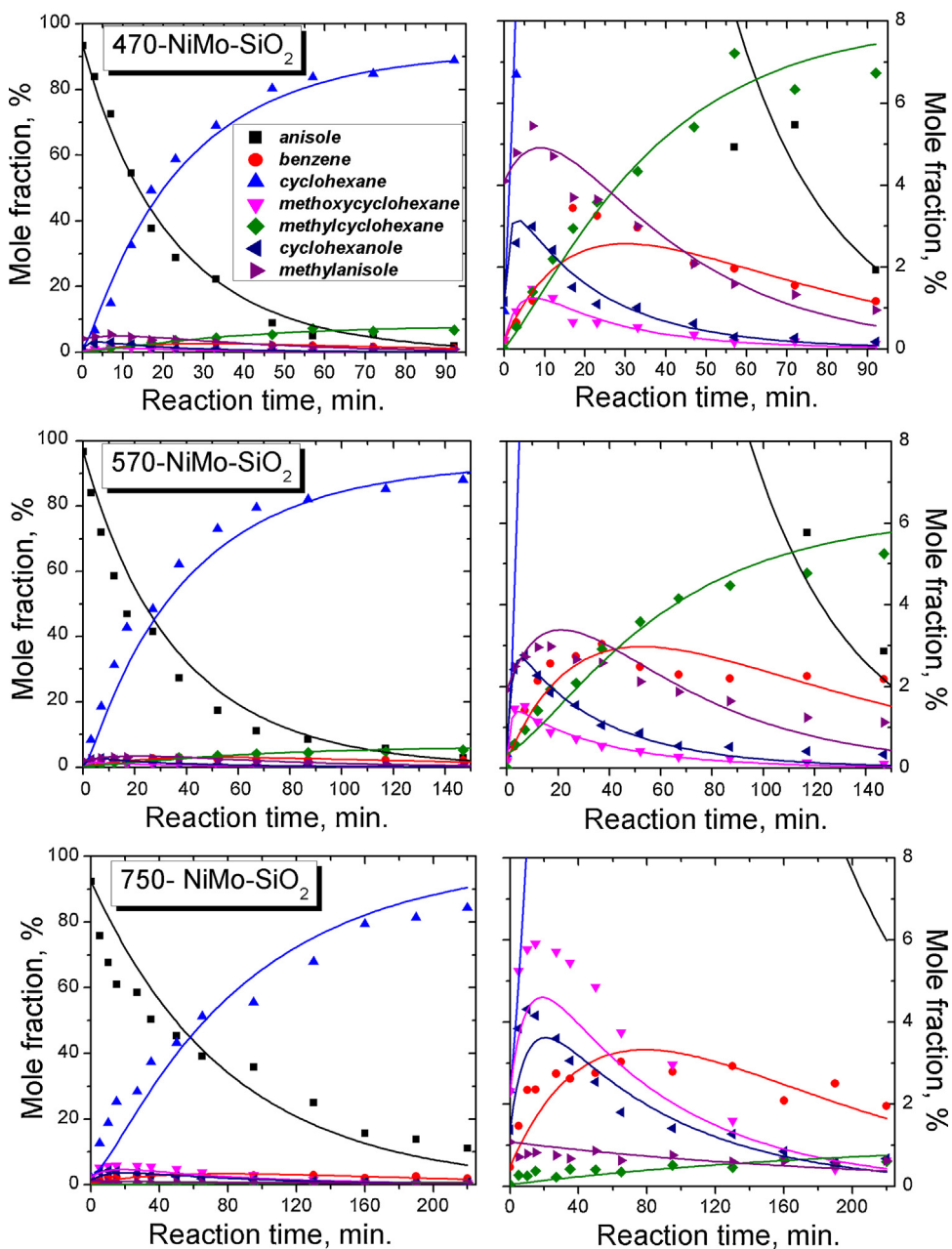


**Fig. 9.** Concentration profiles of the reactant and products as a function of reaction time. Reaction conditions: 300 °C, 6 MPa,  $m_{\text{catalyst}} = 1 \text{ g}$ . The points are experimental data and the lines are calculated from the first-order kinetics model.

**Table 6**

The values of the reaction rate constants for anisole conversion at 300 °C,  $P_{\text{H}_2} = 6 \text{ MPa}$ .

Catalyst	$k_1 (\text{min}^{-1} 10^3)$	$k_2 (\text{min}^{-1} 10^2)$	$k_3 (\text{min}^{-1} 10^2)$	$k_4 (\text{min}^{-1})$	$k_5 (\text{min}^{-1} 10^3)$	$k_6 (\text{min}^{-1})$	$k_7 (1 \text{ min}^{-1} \text{ mol}^{-1} 10^5)$	$k_8 (\text{min}^{-1} 10^2)$
470-NiMo-SiO <sub>2</sub>	$2.4 \pm 0.2$	$2.33 \pm 0.04$	$3.3 \pm 0.1$	$0.99 \pm 0.04$	$5.1 \pm 0.4$	$0.270 \pm 0.002$	$4.01 \pm 0.05$	$3.11 \pm 0.04$
570-NiMo-SiO <sub>2</sub>	$1.57 \pm 0.09$	$1.22 \pm 0.01$	$1.11 \pm 0.02$	$0.78 \pm 0.02$	$12 \pm 1$	$0.74 \pm 0.03$	$2.34 \pm 0.05$	$1.95 \pm 0.05$
750-NiMo-SiO <sub>2</sub>	$1.12 \pm 0.07$	$1.197 \pm 0.006$	$0.27 \pm 0.02$	$0.22 \pm 0.01$	$8.4 \pm 0.2$	$0.13 \pm 0.01$	0	$0.48 \pm 0.02$

**Table 7**

Textural characteristics of the catalyst by CO chemisorption and general and specific activity in HDO and HYD pathway in anisole conversion.  $k_{\text{HDO}} = k_1/m_{\text{cat}}$ ,  $k_{\text{HYD}} = (k_3 + k_5)/m_{\text{cat}}$ ,  $k_{\text{HDO+HYD}} = (k_1 + k_3 + k_5)/m_{\text{cat}}$ ,  $k_i' = k_i m_{\text{cat}}/S_{\text{co}}$ .

Catalyst	$S_{\text{co}} (\text{m}^2/\text{g})$	Average size (nm)	$k_{\text{HDO}} (\text{min}^{-1} \text{ g}^{-1} 10^2)$	$k_{\text{HDO}}' (\text{min}^{-1} \text{ m}^{-2} 10^2)$	$k_{\text{HYD}} (\text{min}^{-1} \text{ g}^{-1} 10^2)$	$k_{\text{HYD}}' (\text{min}^{-1} \text{ m}^{-2} 10^2)$	$k_{\text{HDO+HYD}} (\text{min}^{-1} \text{ g}^{-1} 10^2)$	$k_{\text{HDO+HYD}}' (\text{min}^{-1} \text{ m}^{-2} 10^2)$
470-NiMo-SiO <sub>2</sub>	6.3	106	0.24	0.038	3.81	0.60	4.0	0.64
570-NiMo-SiO <sub>2</sub>	5.4	124	0.157	0.029	2.31	0.43	2.5	0.46
750-NiMo-SiO <sub>2</sub>	0.4	1503	0.112	0.28	1.11	2.775	1.23	3.075

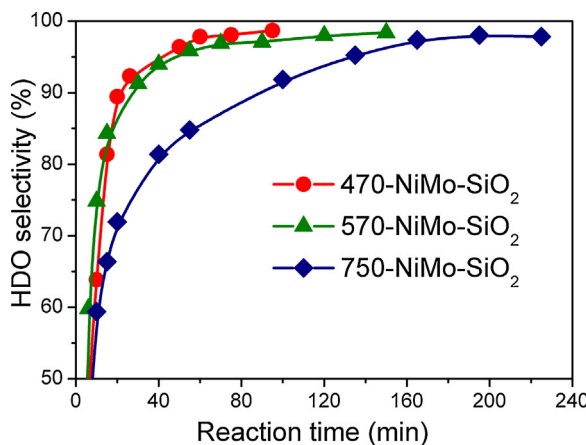


Fig. 10. HDO selectivity of different catalysts.

The HDO selectivity was calculated according to the formula referred to in Section 2.4. The data obtained for the catalyst are shown in Fig. 10. As seen from the picture, the best HDO selectivities were achieved when the NiMoO<sub>4</sub>-SiO<sub>2</sub> system was reduced at 470 and 570 °C. The selectivity is lower for the sample reduced at 750 °C. It is practically in agreement with the values of  $k_{\text{HDO}}$  for all samples. Actually, the HDO selectivity is determined not only by the HDO constant of anisole conversion but also by the sum of all possible pathways. For example, conversion of cyclohexanol ( $k_4$ ) leads to the formation of non-oxygenate cyclohexane, the concentration of which is taken into account in the calculation of the HDO selectivity.

The high HDO selectivity for the 470-NiMo-SiO<sub>2</sub> and 570-NiMo-SiO<sub>2</sub> catalysts can be due to the fact that the surface of these catalysts contains a significant amount of molybdenum in the oxide form. Thus, according to the XRD data, the catalyst contains the MoO<sub>2</sub> and NiMoO<sub>x</sub> particles in which molybdenum may be in different charge states, though the XPS data suggests that the surface of these two samples only contains Mo<sup>4+</sup> whose concentration reaches 32% and 19%, respectively. This, in its turn, leads to a high degree of hydrodeoxygenation as compared to the 750-NiMo-SiO<sub>2</sub> system containing only Mo<sup>0</sup> and Ni<sup>0</sup> [49]. In this case, the 470-NiMo-SiO<sub>2</sub> catalyst demonstrates a higher effective activity and selectivity to oxygen removal due to a higher content of coordinatively unsaturated molybdenum. The effect of a metal oxide on the catalyst activity in oxygen removal is well-described by the Mars–van Krevelen mechanism [50], according to which a reducing agent (hydrogen) adsorbs on the surface of the oxide catalyst and removes the surface oxygen in the form of water, thereby creating a vacancy for the adsorption of oxygen-containing molecules. The second stage is replenishing the oxygen vacancies from the anisole molecule (in this case, with a cleavage of C<sub>ar</sub>–O bond). Also of great importance is the amount of nickel on the catalyst surface, which contributes to the dissociative adsorption of the hydrogen molecule and further spillover of hydrogen from the metal surface onto the molybdenum oxide [51]. This is also a reason for the similar activity and selectivity of catalysts obtained in the reduction of the original sample at 470 and 570 °C, and the ratio Ni/Mo for these two systems is 0.38 and 0.39 compared with the data of XRD showed the ratio Ni/Mo in alloy 0.88 and 0.84, respectively. As noted above, the 750-NiMo-SiO<sub>2</sub> catalyst has the largest specific activity, which indicates a high effect of the spillover as the ratio Ni/Mo for this sample is 0.57.

Thus, it was shown that the reduction temperature of the NiMoO<sub>x</sub> form significantly affects the composition of the products of the hydrogenation of anisole and the selectivity toward oxygen-free products.

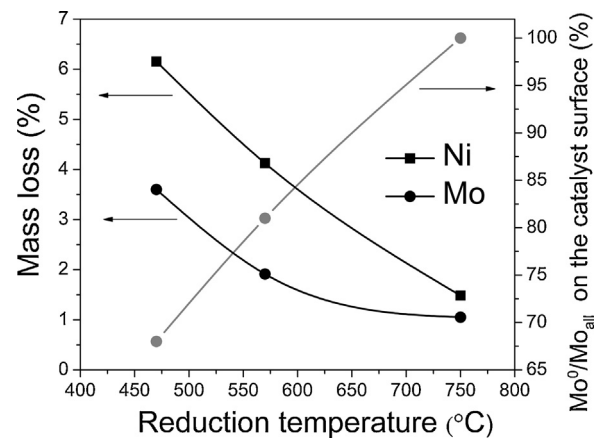


Fig. 11. The dependence of the Ni and Mo mass loss and Mo content on the catalyst surface vs. the catalyst reduction temperature.

### 3.3. The catalysts stability

To determine the corrosion resistance of the catalysts, the reduced forms of the original sample were subjected to desalination in a solution of concentrated acetic acid at 118 °C. As shown by XPS and XRD, the reduction of nickel molybdate causes the formation of the oxide of the NiMoO<sub>x</sub> and MoO<sub>2</sub> compounds within and Ni<sup>0</sup> on the surface of catalysts that can be subjected to the partial dissolution in acetic acid. Fig. 11 shows that the corrosion resistance of the reduced NiMoO<sub>x</sub>-SiO<sub>2</sub> samples (estimated by acetic acid treatment) increases with rising the catalysts reduction temperature, which is accounted for by the increase of Ni-Mo alloys content in the samples. Moreover, it is known that the molybdenum content in the alloy increases along with its corrosion resistance. If the molybdenum content is higher than 15% in the nickel-molybdenum alloy of stands in the solution of mineral acids, the alloy corrosion rate reduces 16 times in 10% HCl at 70 °C with increasing the molybdenum content from 5% to 25% [52]. This explains the small mass loss of the 750-NiMo-SiO<sub>2</sub> sample that contains the Ni<sub>0.79</sub>Mo<sub>0.21</sub> and Ni<sub>3</sub>Mo alloys. In the case of catalysts reduced at 470 and 570 °C alloys and pure molybdenum was observed, nevertheless mass loss value for them was at 2–4 times higher than one was for 750-NiMo-SiO<sub>2</sub>. This may be due to the fact that significant metal dissolution occurs during the reaction of the oxide forms of Ni and Mo with acetic acid. Fig. 11 shows that the catalyst stability increases with increasing of Mo<sup>0</sup> form on the catalyst surface. Thus, when real material with high pH value is used, the 750-NiMo-SiO<sub>2</sub> sample, which also has a very high specific activity, has significant advantage compared to other catalysts.

## 4. Conclusions

The catalytic activity and selectivity of the samples reduced at 470–750 °C in the anisole hydrogenation were studied. The data obtained showed that the most specific activity is possessed by the 750-NiMo-SiO<sub>2</sub> catalyst, which is possibly related to the complete reduction of oxide forms of nickel and molybdenum to the metallic forms having a high activity both in the hydrogen adsorption and the hydrogenation of the C–O bonds and the aromatic ring. In addition to that, the high selectivity in the formation of oxygen-free products is possessed by the catalysts reduced at 470–570 °C, which can be explained by a high content of molybdenum in the form of Mo<sup>4+</sup>. It is also shown that the yield of side products (methylanisoles) decreases with an increase of the reduction temperature. The 750-NiMo-SiO<sub>2</sub> sample is the most stable catalyst, which is due to a high resistance to corrosion of NiMo alloys. Since the

main requirement for the HDO catalyst is the total oxygen removal, which is characterized by HDO selectivity, the most suitable catalysts are the systems reduced at 470 and 570 °C. However, the use of the latter sample provides a decrease in the by-product yield and an increase in the corrosion resistance. Therefore, the catalyst 570-NiMo-SiO<sub>2</sub> is the most effective sample in the HDO process.

## References

- [1] A.V. Bridgwater, D. Meier, D. Radlein, *Org. Geochem.* 30 (1999) 1479–1493.
- [2] C.-L. Lee, D.F. Ollis, *J. Catal.* 87 (1984) 325–331.
- [3] O.I. Senol, T.R. Viljava, A.O.I. Krause, *Catal. Today* 100 (2005) 331–335.
- [4] A.Y. Bunch, Xu, Wang, U.S. Ozkan, *J. Mol. Catal. A* 270 (2007) 264–272.
- [5] C.N. Satterfield, S.H. Yang, *J. Catal.* 81 (1983) 335–346.
- [6] C.-L. Lee, D.F. Ollis, *J. Catal.* 87 (1984) 332–338.
- [7] E.O. Odegbunmi, D.F. Ollis, *J. Catal.* 80 (1983) 65–75.
- [8] E.O. Odegbunmi, D.F. Ollis, *J. Catal.* 80 (1983) 76–89.
- [9] J.B. Bredenbexg, M. Huuska, J. Raty, M. Korpio, *J. Catal.* 77 (1982) 242–247.
- [10] F.E. Massoth, P. Politzer, M.C. Concha, J.S. Murray, J. Jakowski, J. Simons, *J. Phys. Chem. B* 110 (2006) 14283–14291.
- [11] A.R. Ardiyanti, S.A. Khromova, R.H. Venderbosch, V.A. Yakovlev, H.J. Heeres, *Appl. Catal. B* 117–118 (2012) 105–117.
- [12] S.A. Khromova, A.A. Smirnov, O.A. Bulavchenko, A.A. Saraev, V.V. Kaichev, S.I. Reshetnikov, V.A. Yakovlev, *Appl. Catal. A* 470 (2014) 261–270.
- [13] M.V. Bykova, D.Y. Ermakov, S.A. Khromova, A.A. Smirnov, M.Y. Lebedev, V.A. Yakovlev, *Catal. Today* 220–222 (2014) 21–31.
- [14] Y. Xu, T. Wang, L. Ma, Q. Zhang, L. Wang, *Biomass Bioenergy* 33 (2009) 1030–1036.
- [15] S. Mentus, B. Tomić-Tucaković, D. Majstorović, R. Dimitrijević, *Mater. Chem. Phys.* 112 (2008) 254–261.
- [16] J. Court, J.P. Damon, J. Masson, P. Wierzchowski, *Stud. Surf. Sci. Catal.* Ed. J. Barrault C. Bouchoule D. Duprez C. Montassier M. Guisnet and G. Pérot, Elsevier (1988) 189–196.
- [17] Y. Duan, Y. Wu, Q. Zhang, R. Ding, Y. Chen, J. Liu, M. Yang, *J. Mol. Catal. A* 398 (2015) 72–78.
- [18] M.A. Tsurov, P.V. Afanasyev, V.V. Lunin, *Appl. Catal. A* 105 (1993) 205–221.
- [19] J.H. Scofield, *J. Electron Spectrosc. Relat. Phenom.* 8 (1976) 129–137.
- [20] M. Cerro-Alarcón, A. Guerrero-Ruiz, I. Rodríguez-Ramos, *Catal. Today* 93–95 (2004) 395–403.
- [21] A. Guerrero-Ruiz, A. Maroto-Valiente, M. Cerro-Alarcón, B. Bachiller-Baeza, I. Rodríguez-Ramos, *Top. Catal.* 19 (2002) 303–311.
- [22] E. Asedegbega-Nieto, A. Guerrero-Ruiz, I. Rodríguez-Ramos, *Thermochim. Acta* 434 (2005) 113–118.
- [23] A.I. Vagin, N.V. Burmistrova, V.I. Erofeev, *React. Kinet. Catal. Lett.* 28 (1985) 47–52.
- [24] L.M. Madeira, M.F. Portela, C. Mazzocchia, A. Kaddouri, R. Anouchinsky, *Catal. Today* 40 (1998) 229–243.
- [25] M.A. Kipnis, D.A. Agievskii, *Kinet. Catal.* 22 (1981) 1252–1257.
- [26] J.A. Rodriguez, J.-Y. Kim, J.C. Hanson, J.L. Brito, *Catal. Lett.* 82 (2002) 103–109.
- [27] J.L. Brito, J. Laine, K.C. Pratt, *J. Mater. Sci.* 24 (1989) 425–431.
- [28] J.V. Sanders, K.C. Pratt, *J. Catal.* 67 (1981) 331–347.
- [29] J.L. Brito, A.L. Barbosa, A. Albornoz, F. Severino, J. Laine, *Catal. Lett.* 26 (1994) 329–337.
- [30] W.H. McCarroll, L. Katz, R. Ward, *J. Am. Chem. Soc.* 79 (1957) 5410–5414.
- [31] J.A. Rodriguez, S. Chaturvedi, J.C. Hanson, J.L. Brito, *J. Phys. Chem. B* 103 (1999) 770–781.
- [32] L.M. Madeira, M.F. Portela, C. Mazzocchia, A. Kaddouri, R. Anouchinsky, *Catal. Today* 40 (1998) 229–243.
- [33] C.P. Li, A. Proctor, D.M. Hercules, *Appl. Spectrosc.* 38 (1984) 880–886.
- [34] N.V. Kosova, E.T. Devyatkina, V.V. Kaichev, *J. Power Sources* 174 (2007) 735–740.
- [35] D. Alders, F.C. Voogt, T. Hibma, G.A. Sawatzky, *Phys. Rev. B* 54 (1996) 7716–7719.
- [36] N.S. McIntyre, M.G. Cook, *Anal. Chem.* 47 (1975) 2208–2213.
- [37] R.B. Shalvoy, P.J. Reucroft, *J. Catal.* 56 (1979) 336–348.
- [38] M.A. Veenendaal, G.A. Sawatzky, *Phys. Rev. Lett.* 70 (1993) 2459–2462.
- [39] P. Lorenz, J. Finster, G. Wendt, J.V. Salyn, E.K. Zumadilov, V.I. Nefedov, *J. Electron Spectrosc. Relat. Phenom.* 16 (1979) 267–276.
- [40] M.L. Occelli, D. Psaras, S.L. Suib, J.M. Stencel, *Anal. Catal.* 28 (1986) 143–160.
- [41] C.E. Dube, B. Workie, S.P. Kounaves, A. Rabbat, M.L. Aksu, G. Davies, *J. Electron Spectrosc. Relat. Phenom.* 142 (1995) 3357–3365.
- [42] A.F. Carley, S.D. Jackson, J.N. O'shea, M.W. Roberts, *Surf. Sci.* 440 (1999) L868–L874.
- [43] S.J. DeCanio, M.C. Cataldo, E.C. DeCanio, D.A. Storm, *J. Catal.* 119 (1989) 256–260.
- [44] A. Galatyres, S. Wisniewski, J. Grimblot, *J. Electron Spectrosc. Relat. Phenom.* 87 (1997) 31–44.
- [45] C.-O.A. Olsson, H.-J. Mathieu, D. Landolt, *Surf. Interface Anal.* 34 (2002) 130–134.
- [46] C.L. Bianchi, M.G. Cattania, P. Villa, *Appl. Surf. Sci.* 70–71 (1993) 211–216.
- [47] L. Ovari, J. Kiss, A.P. Farkas, F. Solymosi, *J. Phys. Chem. B* 109 (2005) 4638–4645.
- [48] E.O. Odegbunmi, D.F. Ollis, *J. Catal.* 80 (1983) 56–64.
- [49] R.G. Kukushkin, O.A. Bulavchenko, V.V. Kaichev, V.A. Yakovlev, *Appl. Catal. B* 163 (2015) 531–538.
- [50] P. Mars, D.W. Van Krevelen, *Chem. Eng. Sci.* 3 (1954) 41–57.
- [51] W.-Y. Wang, Y.-Q. Yang, J.-G. Bao, H.-A. Luo, *Catal. Commun.* 11 (2009) 100–105.
- [52] I.V. Semenova, G.M. Florianovich, A.V. Khoroshilov, *Corrosion and Corrosion Protection*, Fizmatlit, Moscow, 2002, pp. 336.